Chinese Chemical Letters 36 (2025) 110230

Contents lists available at ScienceDirect

Chinese Chemical Letters

journal homepage: www.elsevier.com/locate/cclet

Two-tailed modification module tuned steric-hindrance effect enabling high therapeutic efficacy of paclitaxel prodrug nanoassemblies

Wenfeng Zang[a,1], Yixin Sun[a,1], Jingyi Zhang[a], Yanzhong Hao[a], Qianhui Jin[a], Hongying Xiao[a], Zuo Zhang[a], Xianbao Shi[b], Jin Sun[a,c], Zhonggui He[a,c], Cong Luo[a,c,*], Bingjun Sun[a,c,*]

[a] Wuya College of Innovation, Shenyang Pharmaceutical University, Shenyang 110016, China
[b] Department of Pharmacy, The First Affiliated Hospital of Jinzhou Medical University, Jinzhou 121000, China
[c] Joint International Research Laboratory of Intelligent Drug Delivery Systems, Ministry of Education, Shenyang 110016, China

ARTICLE INFO

Article history:
Received 22 May 2024
Revised 6 July 2024
Accepted 8 July 2024
Available online 8 July 2024

Keywords:
Prodrug nanoassemblies
Two-tailed modification module
Steric-hindrance
Paclitaxel
Anticancer

ABSTRACT

Self-assembled prodrug nanomedicine has emerged as an advanced platform for antitumor therapy, mainly comprise drug modules, response modules and modification modules. However, existing studies usually compare the differences between single types of modification modules, neglecting the impact of steric-hindrance effect caused by chemical structure. Herein, single-tailed modification module with low-steric-hindrance effect and two-tailed modification module with high-steric-hindrance effect were selected to construct paclitaxel prodrugs (P-LA_{C18} and P-BA_{C18}), and the in-depth insights of the steric-hindrance effect on prodrug nanoassemblies were explored. Notably, the size stability of the two-tailed prodrugs was enhanced due to improved intermolecular interactions and steric hindrance. Single-tailed prodrug nanoassemblies were more susceptible to attack by redox agents, showing faster drug release and stronger antitumor efficacy, but with poorer safety. In contrast, two-tailed prodrug nanoassemblies exhibited significant advantages in terms of pharmacokinetics, tumor accumulation and safety due to the good size stability, thus ensuring equivalent antitumor efficacy at tolerance dose. These findings highlighted the critical role of steric-hindrance effect of the modification module in regulating the structure-activity relationship of prodrug nanoassemblies and proposed new perspectives into the precise design of self-assembled prodrugs for high-performance cancer therapeutics.

Chemotherapy is deemed to be an efficacious modality for clinical cancer therapy [1-5]. Paclitaxel (PTX), one of the most potent natural anticancer drugs, has become the mainstay of cancer chemotherapy regimens. The commercial injection, Taxol, has to incorporate the allergenic excipients Cremophor EL and ethanol to solve the water-solubility of PTX. However, poor tolerance, severe side effects and unsatisfactory pharmacokinetics greatly compromise the therapeutic efficacy of Taxol. Nanomedicines have been shown to improve solubility, extend circulation of blood and enhance tumor accumulation of chemotherapeutics. The most representative PTX nano-formulation, Abraxane, not only solves the water solubility problem of PTX but also increases the tolerated dose of Taxol by about 0.5 times [6,7]. However, lower drug loading, immunogenicity of exogenous albumin, and similar pharmacokinetics to Taxol are still drawbacks of Abraxane. Engineering the innovative PTX nano delivery system to address these dilemmas remains challenging [8,9].

The emergence of self-assembling prodrug nano delivery systems provides an attractive strategy to overcome the above obstacles [10-14]. The prodrugs are capable of self-assembling to form nanostructure after rational design [15-19]. Moreover, prodrug nanoassemblies have ultra-high drug loading owing to the prodrugs acting as both cargoes and carriers [20,21]. In addition, the preparation process of prodrug nanoassemblies is simple and reproducible, which facilitates industrialized scale-up production [22]. However, the rational design of prodrugs is still a concern. For example, paclitaxel-docosahexaenoic acid (PTX-DHA) prodrug significantly reduces the toxic side effects of PTX, increases the maximum tolerated dose by 4 times, and has successfully entered clinical phase III studies [23,24]. However, since PTX and DHA are linked by ester bond, PTX may not be released easily, resulting in

* Corresponding authors.
E-mail addresses: luocong@syphu.edu.cn (C. Luo), sunbingjun_spy@sina.com (B. Sun).
[1] These authors contributed equally to this work.

https://doi.org/10.1016/j.cclet.2024.110230
1001-8417/

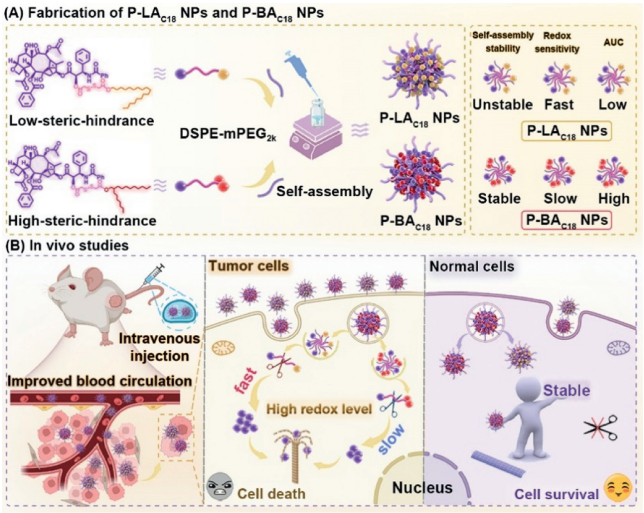

Scheme 1. Two-tailed modification module tuned steric-hindrance effect enabling high therapeutic efficacy of paclitaxel prodrug nanoassemblies.

inferior efficacy. Therefore, the modular design is utilized to divide the prodrug into drug module, response module and modification module [25,26]. Due to the abnormal proliferation and growth of tumors, tumor cells possess higher redox levels than normal cells, which provides favorable opportunities to design redox-responsive modules [27-29]. Disulfide bond has been extensively used as a classical redox response module, and there are a variety of marketed drugs containing disulfide bonds, which have promising application prospects [30-32].

Modification modules usually consist of aliphatic or aromatic structure that facilitate the assembly of the prodrug [33,34]. Paclitaxel, a hydrophobic drug with structural rigidity, is prone to aggregate and precipitate in water. Aliphatic chains can provide steric hindrance to disrupt the ordered arrangement of drug molecules and promote the assembly of prodrugs into stable nanoparticles [35-37]. In general, single-tailed fatty alcohols are widely used as modification modules. Based on the steric-hindrance effect [38,39], we hypothesized that two-tailed fatty alcohols may provide stronger steric-hindrance, which affects the assembly mechanism, drug release characteristics and therapeutic efficacy of the prodrug nanoassemblies. Therefore, exploring the action mechanism of different types of modification modules is conducive to resolving the structure-activity relationship of the prodrug nanoassemblies.

Herein, single- and two-tailed modification chains were selected for the construction of PTX prodrug nanoassemblies. The two-tailed modified prodrugs exhibited better size stability as the two-tailed modification module provided higher steric-hindrance. However, the steric-hindrance effect also impeded the attack of redox agents, resulting in a lower redox sensitivity of the two-tailed modified prodrug nanoassemblies. The single-tailed modified prodrug nanoassemblies exhibited higher redox sensitivity, which released more PTX at the tumor site with better antitumor efficacy. The two-tailed modified prodrug nanoassemblies displayed more advantages in terms of pharmacokinetics and tumor accumulation due to better colloidal stability. In addition, the antitumor effectiveness and safety of the two-tailed modified prodrug nanoassemblies were optimized due to the balance of multiple influencing factors (Scheme 1). Therefore, by investigating the steric-hindrance effect of modification modules, this study proposed new perspectives into the rational design of prodrug nanoassemblies.

To investigate the potential mechanism of the steric-hindrance effect on the behavior of prodrug nanoassemblies, prodrugs were constructed by linking PTX and modification modules with disulfide bonds. Single-tailed 1-octadecanol and two-tailed 2-heptylundecanol were selected as modification modules, and the prodrugs were named P-LA$_{C18}$ and P-BA$_{C18}$. The synthetic pathways were illustrated in Fig. S1 (Supporting information). The structures of P-LA$_{C18}$ and P-BA$_{C18}$ were verified using nuclear magnetic resonance hydrogen spectroscopy and mass spectrum (Figs. S2 and S3 in Supporting information). The purities of P-LA$_{C18}$ and P-BA$_{C18}$ were all above 99%, which were determined by high performance liquid chromatography (HPLC) (Figs. S2 and S3).

To explore the self-assembly ability, non-PEGylated P-LA$_{C18}$ and P-BA$_{C18}$ nanoparticles (NPs) were prepared. The prodrugs could self-assemble to form nanoassemblies at the concentrations of 0.1, 0.2 and 0.4 mg/mL. Among them, the particle size of non-PEGylated P-BA$_{C18}$ NPs was smaller (Table S1 in Supporting information). When the concentration increased to 0.6 mg/mL, P-LA$_{C18}$ precipitated in deionized water (Fig. 1A, Fig. S4 and Table S1 in Supporting information), while the P-BA$_{C18}$ NPs exhibited uniform particle size distribution. In addition, the stability of non-PEGylated P-LA$_{C18}$ and P-BA$_{C18}$ NPs was investigated under room temperature. From day 8, the particle size of non-PEGylated P-LA$_{C18}$ NPs gradually grew, while non-PEGylated P-BA$_{C18}$ NPs remained unchanged (Fig. S5 in Supporting information). Therefore, the two-tailed modified prodrug nanoassemblies (P-BA$_{C18}$ NPs) displayed superior size stability.

The self-assembly mechanism of the prodrugs was studied to explore the factors contributing to the enhanced assembly capacity of the two-tailed P-BA$_{C18}$ NPs. The Log*P* values of P-LA$_{C18}$ and P-BA$_{C18}$ were 12.05 and 12.35, suggesting that the hydrophobic interactions of P-BA$_{C18}$ might be stronger than P-LA$_{C18}$ (Fig. 1E). In addition, non-PEGylated prodrug nanoassemblies were co-incubated with NaCl (shielding of electrostatic interactions), sodium dodecyl sulfate (SDS, shielding of hydrophobic interaction) and urea (shielding of hydrogen bonds) to validate the intermolecular forces. As shown in Fig. 1B, the particle size of the non-PEGylated prodrug nanoassemblies was significantly increased, indicating that three forces were involved in the assembly of the prodrugs. Notably, the particle size of non-PEGylated P-BA$_{C18}$ NPs was changed remarkably, suggesting that the assembly process might involve stronger intermolecular forces.

However, too strong hydrophobic forces could lead to aggregation between molecules. Aliphatic chains provided steric-hindrance to disrupt the ordered arrangement of drug molecules. Thus, the steric-hindrance of the prodrugs was simulated. In addition, volume calculations were performed using Yasara, with P-BA$_{C18}$ (3092.70 Å^3) > P-LA$_{C18}$ (3069.50 Å^3), suggesting that P-BA$_{C18}$ might possess stronger steric-hindrance (Fig. 1C). Then, the binding energies and intermolecular forces were calculated using molecular simulations. The binding free energy was as follows: P-BA$_{C18}$ NPs (−2.8 kcal/mol) and P-LA$_{C18}$ NPs (−1.9 kcal/mol). The relatively lower binding energy value of P-BA$_{C18}$ NPs signified heightened size stability (Fig. 1D). The above results revealed that the composition of the modification modules had a substantial impact on the assembly mechanism and size stability of the prodrugs. Our previous study found that modification modules could provide structural defects to facilitate the assembly of prodrugs. Branched-chain fatty alcohols could provide greater steric hindrance for prodrugs to balance intermolecular forces, which was expected to improve assembly capacity. The smaller particle size of P-BA$_{C18}$ NPs suggested the possibility of forming more compact nanostructures and the non-PEGylated P-BA$_{C18}$ NPs also displayed better assembly capacity. In addition, transmission electron microscope (TEM) showed that prodrug nanoassemblies were spherical with no significant difference in morphology (Fig. S6 in Supporting information).

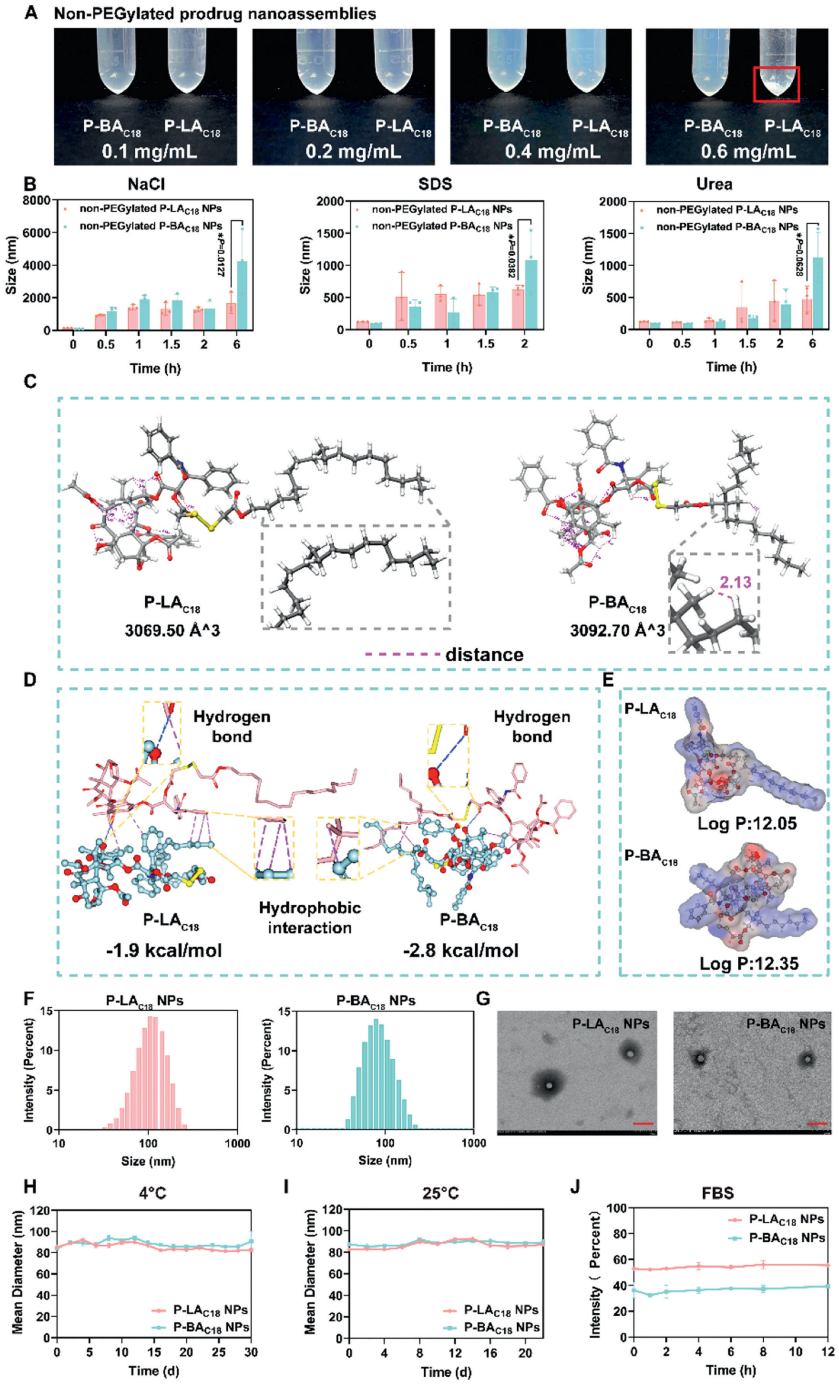

Fig. 1. Self-assembly capacity and characterization of prodrug nanoassemblies. (A) The appearance of non-PEGylated P-LA$_{C18}$ NPs and P-BA$_{C18}$ NPs at concentrations of 0.1, 0.2, 0.4 and 0.6 mg/mL. (B) The variation of the particle size of non-PEGylated prodrug nanoassemblies after co-incubated with NaCl, SDS or Urea. (C) Steric-hindrance effects of P-LA$_{C18}$ and P-BA$_{C18}$. (D) Intermolecular interactions of P-LA$_{C18}$ NPs and P-BA$_{C18}$ NPs during the self-assembly process. (E) Log*P* values of two prodrugs. (F) The particle size and (G) morphology of P-LA$_{C18}$ NPs and P-BA$_{C18}$ NPs. Scale bar: 200 nm. Storage stability of P-LA$_{C18}$ NPs and P-BA$_{C18}$ NPs (H) at 4 °C and (I) at 25 °C. (J) The changes in particle size of P-LA$_{C18}$ NPs and P-BA$_{C18}$ NPs after coincubation with PBS containing FBS for 12 h. Data are presented as mean ± SD ($n = 3$). $^*P < 0.05$ by two-tailed Student's *t*-test.

DSPE-mPEG$_{2K}$ modification could prolong the systemic circulation of the prodrug nanoassemblies by reducing the uptake of the mononuclear phagocytic system (MPS). Therefore, PEGylated P-LA$_{C18}$ NPs and P-BA$_{C18}$ NPs were prepared, named P-LA$_{C18}$ NPs and P-BA$_{C18}$ NPs (Fig. S7A in Supporting information). A significant increase in the particle size of the prodrug nanoassemblies was observed only in the presence of SDS, and the change in the particle size of the P-BA$_{C18}$ NPs was more dramatic (Fig. S7B in Supporting information). Thus, hydrophobic force might be the primary force driving the assembly of prodrugs. The particle size of P-BA$_{C18}$ NPs and P-LA$_{C18}$ NPs were 86.5 and 105.6 nm, respectively. The particle size distribution was uniform, with the poly dispersity index (PDI) less than 0.2 (Fig. 1F and Table S2 in Supporting information). In addition, the P-BA$_{C18}$ NPs possessed a lower zeta potential of approximately −28 mV (Table S2), which could prevent the aggregation of the nanoassemblies. Moreover, the drug loading of the prodrug nanoassemblies was greater than 50%. Both prodrug nanoassemblies showed uniform spher-

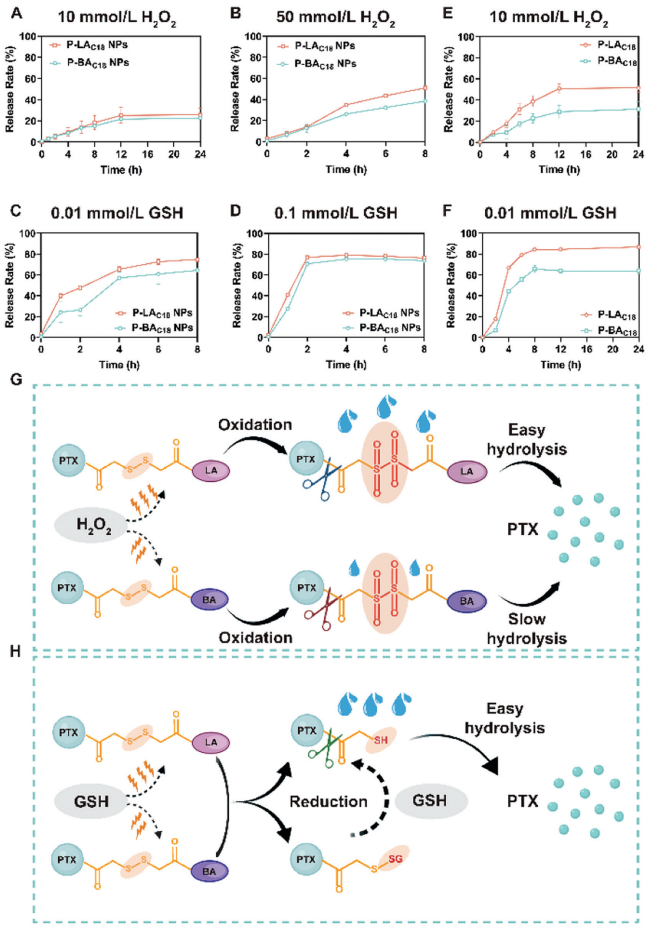

Fig. 2. Redox dual-sensitive drug release. The drug release profiles of P-LA_{C18} NPs and P-BA_{C18} NPs were measured under the following conditions: (A) 10 mmol/L H_2O_2; (B) 50 mmol/L H_2O_2; (C) 0.01 mmol/L GSH; (D) 0.1 mmol/L GSH. Redox dual-sensitive drug release of prodrugs in (E) 10 mmol/L H_2O_2 and (F) 0.01 mmol/L GSH. (G) The oxidization mechanism and (H) the reduction mechanism of P-LA_{C18} NPs and P-BA_{C18} NPs. Data are presented as mean ± SD ($n = 3$).

ical structures as observed by transmission electron microscopy (Fig. 1G).

As shown in Figs. 1H and I, P-BA_{C18} NPs and P-LA_{C18} NPs exhibited good stability at 4 °C (30 days) and room temperature (22 days). In addition, the prodrug nanoassemblies exhibited negligible changes in particle size following co-incubation with phosphate buffered solution (PBS, pH 7.4) supplemented with 10% fetal bovine serum (FBS) for 12 h, demonstrating the excellent colloidal stability (Fig. 1J). As shown in Fig. S8 (Supporting information), the particle size of prodrug nanoassemblies gradually increased after co-incubation with plasma, and the particle size of P-LA_{C18} NPs increased significantly at 1 h. In contrast, P-BA_{C18} NPs showed good colloidal stability.

The impact of steric-hindrance effect on the redox reactivity of P-LA_{C18} NPs and P-BA_{C18} NPs was investigated using hydrogen peroxide (H_2O_2) and glutathione (GSH) as triggering agents. As shown in Fig. S9 (Supporting information), little PTX was released from P-LA_{C18} NPs and P-BA_{C18} NPs in the blank medium without the addition of H_2O_2 and GSH. In the presence of H_2O_2, the release of the prodrug nanoassemblies showed concentration- and time-dependence. The release of P-LA_{C18} NPs was greater than that of P-BA_{C18} NPs regardless of the concentration of H_2O_2 (Figs. 2A and B). In addition, the prodrug solution was added to the release medium containing 10 mmol/L H_2O_2 and 0.01 mmol/L GSH. In this case, the release difference between P-LA_{C18} and P-BA_{C18} was more significant (Figs. 2E and F). Therefore, the redox sensitivity was mainly affected by the molecular conformation of the prodrugs, but the release trend was consistent with prodrug nanoassemblies. To investigate the underlying mechanism, the oxidative release mechanism of P-LA_{C18} NPs and P-BA_{C18} NPs was examined. As shown in Fig. 2G, the disulfide bonds could be oxidized to sulfoxide or sulfone, which increased the hydrophilicity of the system and facilitated the hydrolysis of adjacent ester bonds and the release of PTX. Compared with the single-tailed modification module, the increased steric-hindrance effect of the two-tailed modification module hindered the attack of H_2O_2 on the sulfur atoms and ester bonds, and the oxidative sensitivity of the P-BA_{C18} NPs was weaker than P-LA_{C18} NPs. The oxidation intermediates were captured using ultra performance liquid chromatography tandem mass spectrometry (UPLC-MS-MS) (Figs. S10 and S12 in Supporting information).

As shown in Figs. 2C and D, the reduction sensitivity of P-BA_{C18} NPs remained weaker than that of P-LA_{C18} NPs in the presence of GSH. The mechanism was that the disulfide bond was cleaved to generate hydrophilic thiols, which further enhanced the hydrophilicity of the system and facilitated the hydrolysis of neighboring ester bonds (Fig. 2H). Despite having identical intermediates (Figs. S11 and S13 in Supporting information), the steric-hindrance effect of the two-tailed modification module was greater than the single-tailed modification module, which led to differences in the attack of GSH on the disulfide bonds.

The effective release of the parent drug was essential for ensuring the potent antitumor efficacy of the prodrug nanoassemblies. Thus, the intracellular drug release was examined. The release of PTX from the prodrug nanoassemblies was delayed compared to that of Taxol and Abraxane. Additionally, P-LA_{C18} NPs demonstrated a higher PTX release compared to P-BA_{C18} NPs, which was consistent with the *in vitro* release results (Figs. 3A–C).

Subsequently, the cytotoxicity of P-LA_{C18} NPs and P-BA_{C18} NPs was evaluated against two tumor cell lines (4T1 and A549) and one normal cell line (3T3). As shown in Fig. 3D and E, Figs. S14A and B and Table S3 (Supporting information), the delayed release of PTX resulted in lower cytotoxicity of P-LA_{C18} NPs and P-BA_{C18} NPs compared to Taxol and Abraxane. Moreover, the cytotoxicity of the P-LA_{C18} NPs was stronger than P-BA_{C18} NPs, which may be attributed to more PTX release from P-LA_{C18} NPs within the tumor redox microenvironment (Figs. 3D and E).

The cytotoxicity of the formulations was decreased for normal cells, especially for the prodrug nanoassemblies (Fig. 3F and Fig. S14C in Supporting information). To accurately demonstrate the tumor selectivity of P-LA_{C18} NPs and P-BA_{C18} NPs, the tumor selectivity index (SI) was calculated as shown in Table S4 (Supporting information). P-LA_{C18} NPs and P-BA_{C18} NPs exhibited higher tumor selectivity compared with Taxol and Abraxane. P-LA_{C18} NPs and P-BA_{C18} NPs released more PTX in the high redox microenvironment of tumor cells and reduced toxicity to normal cells (Fig. 3G). Moreover, P-BA_{C18} NPs exhibited the highest tumor selectivity, which might show superior safety.

P-LA_{C18} NPs and P-BA_{C18} NPs were co-incubated with fresh rat plasma to investigate the plasma stability. As shown in Fig. S15 (Supporting information), P-BA_{C18} NPs had more undegraded prodrugs compared to P-LA_{C18} NPs. The better plasma stability of the two-tailed prodrug nanoassemblies (P-BA_{C18} NPs) was due to the improved size stability. Moreover, the biosafety of the prodrug nanoassemblies was further demonstrated by hemolysis assay before the *in vivo* studies. Neither of the prodrug nanoassemblies caused hemolysis in the range of 0.5–2 mg/mL, and the hemolysis percentage (HP%) was less than 5%, which demonstrated the safety of intravenous administration (Figs. S16A–D in Supporting information).

Pharmacokinetic studies were conducted to investigate the influence of steric-hindrance on the *in vivo* behavior of P-LA_{C18} NPs

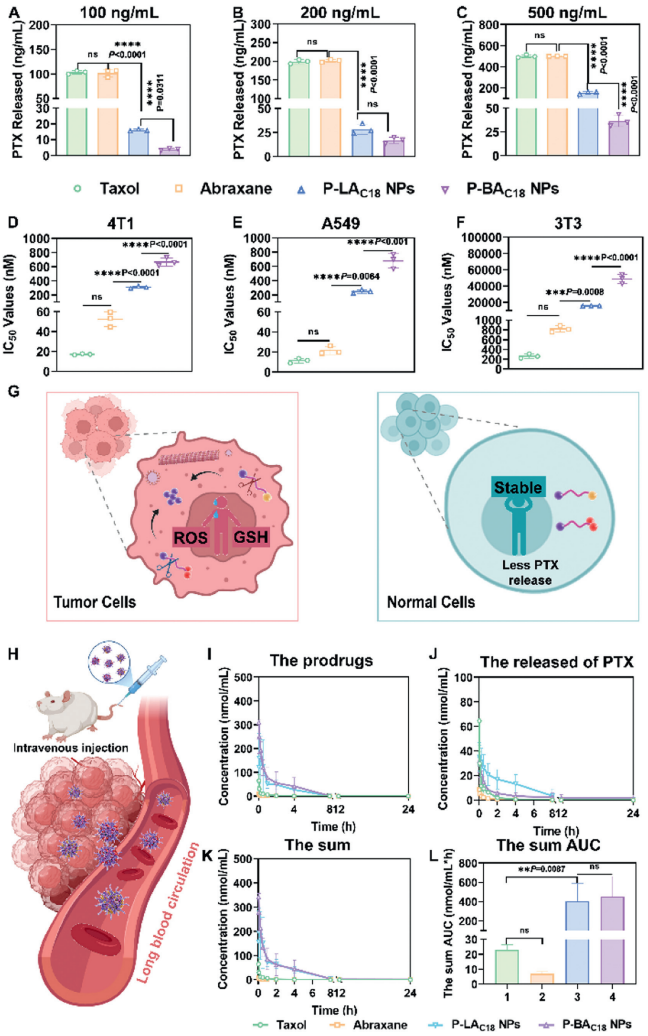

Fig. 3. Cell assays and pharmacokinetics of P-LA$_{C18}$ NPs and P-BA$_{C18}$ NPs. PTX released from different concentrations of P-LA$_{C18}$ NPs and P-BA$_{C18}$ NPs, including 100 ng/mL (A), 200 ng/mL (B) and 500 ng/mL (C). The IC$_{50}$ values of Taxol, Abraxane, P-LA$_{C18}$ NPs and P-BA$_{C18}$ NPs in 4T1 cells (D), A549 cells (E) and 3T3 cells (F) were determined. Data are presented as mean ± SD ($n = 3$). (G) Schematic representation of the tumor-selective cytotoxicity of P-LA$_{C18}$ NPs and P-BA$_{C18}$ NPs. (H) P-LA$_{C18}$ NPs and P-BA$_{C18}$ NPs were present in the systemic circulation. The AUC$_{0-24\,h}$ of the (I) prodrugs, (J) the released PTX, and (K) the sum (prodrug and PTX, PTX equivalent). (L) The AUC$_{0-24\,h}$ of the sum (prodrugs and PTX, PTX equivalent). Data are presented as mean ± SD ($n = 5$). n.s., no significance. $^{**}P < 0.01$, $^{***}P < 0.001$, $^{****}P < 0.0001$ by two-tailed Student's *t*-test.

and P-BA$_{C18}$ NPs. All experimental procedures were carried out in strict compliance with the protocols for animal testing and received approval from the Institutional Animal Ethics Committee (IAEC) of Shenyang Pharmaceutical School. The concentration-time profiles of the prodrugs, released PTX and the sum of both them were depicted in Figs. 3I–K. Taxol was cleared quickly from the circulatory system, with a half-life of only 2.2 h (Table S5 in Supporting information). In contrast, the prodrug nanoassemblies extended the duration of blood circulation. (Fig. 3H and Table S5). In addition, the area under the curve (AUC) of P-BA$_{C18}$ NPs and P-LA$_{C18}$ NPs were approximately 20 and 19 times higher than Taxol (Fig. 3L), respectively. For the prodrug nanoassemblies, a minimal amount of free PTX was released from P-BA$_{C18}$ NPs compared to P-LA$_{C18}$ NPs. This might be due to the stronger redox sensitivity of P-LA$_{C18}$ NPs and the presence of some oxidizing substances within the circulatory system, such as oxygen, leading to the release of PTX from P-LA$_{C18}$ NPs. In comparison, P-BA$_{C18}$ NPs exhibited superior pharmacokinetic behavior due to appropriate redox sensitivity and better size stability.

The positive antitumor efficacy of the prodrug nanoassemblies relied on elevated tumor accumulation and effective drug release. Therefore, an examination of the biodistribution and tumor accumulation of the prodrug nanoassemblies were conducted (Fig. S17 in Supporting information). Notably, P-BA$_{C18}$ NPs displayed the highest tumor accumulation (Fig. S17F). In addition, the prodrug of single-tailed modified P-LA$_{C18}$ NPs was completely degraded at 4 h, and PTX was gradually eliminated at 8 h. However, the prodrug of two-tailed modified P-BA$_{C18}$ NPs could still be detected at 8 h, and the release of PTX increased with time. In addition, similar results were found in the *in vivo* imaging in mice (Fig. S17H). The higher tumor accumulation and sustained PTX release contributed to the excellent pharmacodynamics and safety of the two-tailed modified prodrug nanoassemblies.

Next, orthotopic breast cancer model (4T1) was developed (Fig. 4A). As shown in Fig. 4B and Fig. S18A (Supporting information), P-LA$_{C18}$ NPs and Taxol showed excellent tumor growth inhibition. In addition, the tumor burden of P-LA$_{C18}$ NPs group was the lowest (Fig. 4D), which could be attributed to the higher redox release capacity and good tumor selectivity. P-BA$_{C18}$ NPs showed weaker tumor growth inhibition than P-LA$_{C18}$ NPs and Taxol, but similar to Abraxane. Moreover, lung metastasis was significantly inhibited in the prodrug nanoassemblies groups (Fig. 4E and Fig. S18B in Supporting information). The tumor tissues of the administered groups showed obvious cell necrosis (Fig. 4F). The terminal dUTP nick end labeling (TUNEL) (Figs. S19B and C in Supporting information) and Ki-67 staining (Figs. S19D and E in Supporting information) also showed that P-LA$_{C18}$ NPs induced higher levels of tumor apoptosis and inhibited tumor proliferation.

To further validate the antitumor efficacy of P-LA$_{C18}$ NPs and P-BA$_{C18}$ NPs in different tumor models and at different administered doses, A549 tumor-bearing nude mice were constructed (Fig. 4G). As shown in Figs. 4H and J, at low doses, the P-LA$_{C18}$ NPs exhibited the smallest tumor volume due to the fastest release of PTX. The antitumor effect of P-BA$_{C18}$ NPs was slightly weaker than P-LA$_{C18}$ NPs. At high doses, the tumor growth inhibition of P-BA$_{C18}$ NPs was comparable to P-LA$_{C18}$ NPs. The enhanced antitumor effect of P-BA$_{C18}$ NPs was ascribed to good colloidal stability, improved pharmacokinetics and high tumor accumulation.

To evaluate the safety of P-LA$_{C18}$ NPs and P-BA$_{C18}$ NPs, changes in body weight of the mice were monitored during the pharmacodynamic experiments. In the breast cancer model, mice in the Taxol group experienced greater weight loss compared with the saline group (Fig. 4C). No significant body weight change was observed in other preparation groups. At the end of the pharmacodynamic experiment, the tissues from each group were stained with hematoxylin-eosin (H&E) staining. Hepatic edema and hemorrhage were seen in the Taxol group (Fig. S19A in Supporting information). Blood cell analysis revealed lower Gran% values in the Taxol group, indicating higher toxic side effects (Figs. S20A–D in Supporting information). In the lung cancer model, mice in the Abraxane group showed slight weight loss at different administered doses. In addition, mice in the P-LA$_{C18}$ NPs group showed significant weight loss and death when administered at doses of 30 mg/kg and 60 mg/kg (Figs. 4I and K). The body weight of mice in the P-BA$_{C18}$ NPs group showed no significant change at both low and high doses, indicating a favorable safety.

Subsequently, the tolerance of P-LA$_{C18}$ NPs and P-BA$_{C18}$ NPs was assessed in BALB/c-nude mice, using body weight and survival rate as indicators. As shown in Figs. S20E and F and Table S6 (Supporting information), the tolerance of P-LA$_{C18}$ NPs was poor, and all mice died on the 6th day with continuous weight loss. Similarly, mice in the Abraxane group showed poor tolerance with the same weight loss and death after continuous administration. In contrast,

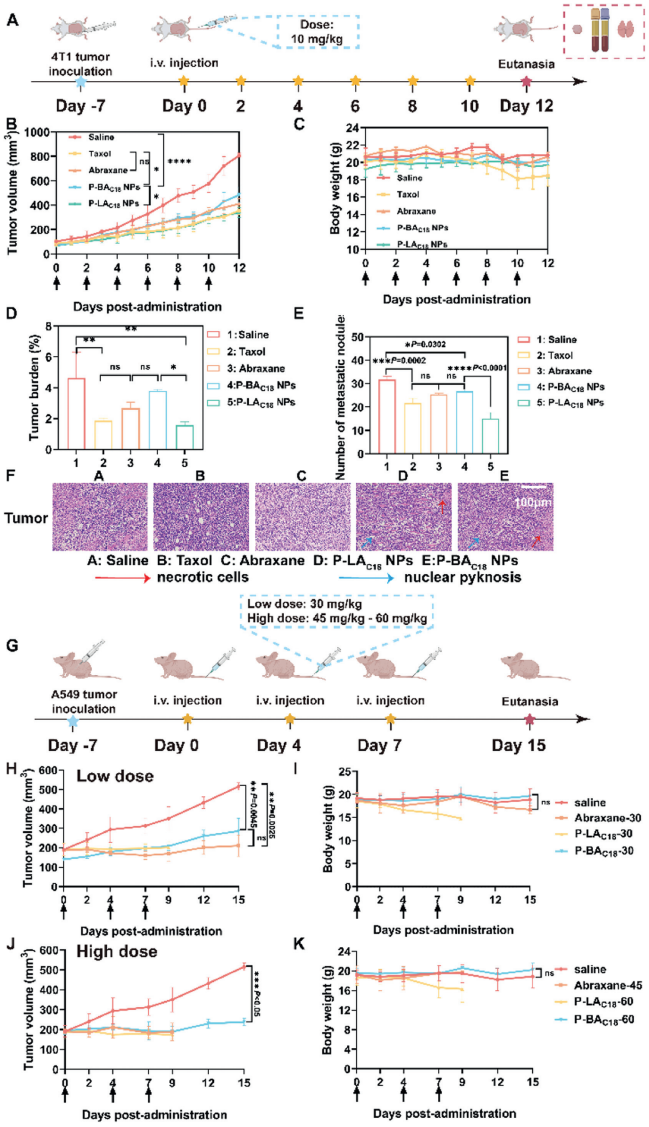

Fig. 4. Antitumor efficacy of P-LA_{C18} NPs and P-BA_{C18} NPs. (A) Antitumor effects against orthotopic 4T1 tumors. (B–D) Tumor growth kinetics, body weight changes, and tumor burden were evaluated in BALB/c mice at a dose of 10 mg/kg. (E) The number of metastatic nodules. (F) H&E staining of tumor sections of 4T1 tumor-bearing mice. Scale bar: 100 μm. (G) Schematic of the administration schedule in A549 xenograft tumors. (H, I) Tumor growth profiles and body weight at 30 mg/kg. (J, K) Tumor growth profiles and body weight at 45 mg/kg of Abraxane, and 60 mg/kg of prodrug nanoassemblies. Data are presented as mean ± SD ($n = 3$). $^{*}P < 0.05$, $^{**}P < 0.01$, $^{***}P < 0.001$, $^{****}P < 0.0001$ by one-way analysis of variance (ANOVA).

mice in P-BA_{C18} NPs group demonstrated no significant abnormalities in body weight, indicating an outstanding tolerance.

In this study, the disulfide bond-bridged single-tailed and two-tailed modified prodrug nanoassemblies (P-LA_{C18} NPs and P-BA_{C18} NPs) were constructed, and the steric-hindrance effect of the two-tailed modification module was found to significant impact the formulation properties and therapeutic index of the prodrug nanoassemblies. Firstly, the two-tailed modified prodrug nanoassemblies exhibited lower binding energy and stronger intermolecular forces, which promoted the stable assembly P-BA_{C18} NPs. Secondly, in comparison to the single-tailed prodrug nanoassemblies, the redox sensitivity of the two-tailed prodrug nanoassemblies was reduced due to the steric-hindrance effect. Finally, due to the favorable size stability and appropriate redox sensitivity, the two-tailed modified prodrug nanoassemblies showed advantages in pharmacokinetics, biodistribution, pharmacodynamics and safety. The single-tailed modified prodrug nanoassemblies showed impressive antitumor effects due to rapid PTX release, but the safety remained to be a concern. Our findings shed light on the relationship between steric-hindrance effects and the activities of the prodrug nanoassemblies, and offered new viewpoints into the rational design of self-assembled prodrugs for high performance cancer therapeutics.

Declaration of competing interest

The authors declare that they have no known competing financial interests or personal relationships that could have appeared to influence the work reported in this paper.

CRediT authorship contribution statement

Wenfeng Zang: Writing – original draft, Methodology, Investigation. **Yixin Sun:** Writing – original draft, Methodology, Investigation. **Jingyi Zhang:** Data curation. **Yanzhong Hao:** Methodology, Formal analysis. **Qianhui Jin:** Data curation. **Hongying Xiao:** Validation, Supervision. **Zuo Zhang:** Validation, Supervision. **Xianbao Shi:** Validation, Supervision. **Jin Sun:** Writing – review & editing, Funding acquisition. **Zhonggui He:** Writing – review & editing, Funding acquisition. **Cong Luo:** Writing – review & editing. **Bingjun Sun:** Writing – review & editing, Funding acquisition, Data curation.

Acknowledgments

This work was financially supported by the National Natural Science Foundation of China, (Nos. 82272151, 82204318), Liaoning Revitalization Talents Program (No. XLYC2203083), and Shenyang Young and Middle-aged Science and Technology Innovation Talent Support Program (No. RC220389), Postdoctoral Fellowship Program of CPSF (No. GZC20231732), China Postdoctoral Science Foundation (Nos. 2023TQ0222, 2023MD744229).

Supplementary materials

Supplementary material associated with this article can be found, in the online version, at doi:10.1016/j.cclet.2024.110230.

References

[1] C. Swanton, E. Bernard, C. Abbosh, et al., Cell 187 (2024) 1589–1616.
[2] J. Shi, P.W. Kantoff, R. Wooster, et al., Nat. Rev. Cancer 17 (2016) 20–37.
[3] R. Walther, J. Rautio, A.N. Zelikin, Adv. Drug Deliv. Rev. 118 (2017) 65–77.
[4] B. Sun, C. Luo, W. Cui, et al., J. Control. Release 264 (2017) 145–159.
[5] Q. Song, Y. Yin, L. Shang, et al., Nano Lett. 17 (2017) 6366–6375.
[6] Q. Chen, Z. Liu, Adv. Mater. 28 (2016) 10557–10566.
[7] M. Hama, Y. Ishima, V.T.G. Chuang, et al., ACS Appl. Mater. Interfaces 13 (2021) 19736–19744.
[8] F. Kratz, J. Control. Release 190 (2014) 331–336.
[9] S. Ezrahi, A. Aserin, N. Garti, Adv. Colloid Interface Sci. 263 (2019) 95–130.
[10] B. Sun, C. Luo, H. Yu, et al., Nano Lett. 18 (2018) 3643–3650.
[11] C.M. Hartshorn, M.S. Bradbury, G.M. Lanza, et al., ACS Nano 12 (2017) 24–43.
[12] J. Wang, B. Li, U.B. Kompella, et al., MedComm Biomater. Appl. 2 (2023) e30.
[13] T. Tong, L. Chen, S. Wu, et al., Chin. Chem. Lett. 35 (2024) 109689.
[14] S. Li, Y. Yang, S. Wang, et al., Exploration 2 (2022) 20210223.
[15] Y. Huang, T. Wang, Q. Tan, et al., Int. J. Nanomed. Volume 16 (2021) 4117–4146.
[16] J. Li, Y. Li, Y. Wang, et al., Nano Lett. 17 (2017) 6983–6990.
[17] X. Wu, X. Chen, X. Wang, et al., Chin. Chem. Lett. 35 (2024) 108756.
[18] R. Zhang, X. You, M. Luo, et al., Carbohydr Polym. 292 (2022) 119695.
[19] W. Zhong, X. Zhang, X. Duan, et al., Acta Biomater. 144 (2022) 67–80.
[20] L. Li, B. Sun, J. Sun, et al., Chin. Chem. Lett. 35 (2024) 109538.
[21] H. Liu, T. Nie, X. Duan, et al., J. Control. Release 359 (2023) 132–146.
[22] J. Zhang, H. Guo, M. Liu, et al., Exploration 4 (2024) 20230087.
[23] C. Zhang, Y. Zuo, T. Zhang, et al., Acta Mater. Med. 2 (2023) 430–448.
[24] R. Wang, X. Zhang, K. Feng, et al., Asian J. Pharm. Sci. 18 (2023) 100857.
[25] C. Luo, J. Sun, B. Sun, et al., Small 12 (2016) 6353–6362.
[26] B. Li, T. Tan, W. Chu, et al., Drug Deliv. 29 (2021) 75–88.
[27] X. Wang, T. Liu, Y. Huang, et al., Nanoscale Horiz. 8 (2023) 235–244.

[28] Q. Pei, B. Jiang, D. Hao, et al., Acta Pharmacol. Sin. B 13 (2023) 3252–3276.
[29] Y. Li, Q. Bao, S. Yang, et al., View 3 (2022) 20200027.
[30] J. Zhang, Y. Zhang, Y. Huang, et al., Chem. Eng. J. 458 (2023) 141510.
[31] L. Li, S. Zuo, F. Dong, et al., Asian J. Pharm. Sci. 16 (2021) 337–349.
[32] C. Luo, B. Sun, C. Wang, et al., J. Control. Release 302 (2019) 79–89.
[33] Y. Sun, S. Wang, Y. Li, et al., Acta Biomater. 157 (2023) 417–427.
[34] Y. Gao, S. Zuo, L. Li, et al., Nanoscale 13 (2021) 10536–10543.
[35] H. Xu, S. Zuo, D. Wang, et al., J. Control. Release 360 (2023) 784–795.
[36] Y. Yang, X. Li, J. Song, et al., Nano Lett. 23 (2023) 1530–1538.
[37] G. Li, F. Xia, H. Xiao, et al., Nano. Res. 17 (2023) 2908–2918.
[38] G. Wang, Q. Bai, H. Liu, et al., Inorg. Chem. 62 (2023) 6537–6543.
[39] J. Liao, S. Liu, Y. Yuan, et al., New J. Chem. 42 (2018) 5698–5708.